

# The chiral random walk: A quantum-inspired framework for odd diffusion

Jan Wójcik<sup>1, 2, \*</sup> and Erik Kalz<sup>3, †</sup>

<sup>1</sup>*Institute of Theoretical Physics and Astrophysics, University of Gdańsk, 80-308 Gdańsk, Poland*

<sup>2</sup>*Institute of Spintronics and Quantum Information, Faculty of Physics and Astronomy,  
Adam Mickiewicz University, 61-614 Poznań, Poland*

<sup>3</sup>*Institute of Physics and Astronomy, University of Potsdam, 14476 Potsdam, Germany*

Chirality in active and passive fluids gives rise to *odd* transport properties, most notably the emergence of robust edge currents that defy standard dissipative dynamics. While these phenomena are well-described by continuum hydrodynamics, a microscopic framework connecting them to their topological origins has remained elusive. Here, we present a lattice model for an isotropic chiral random walk that bridges the gap between classical stochastic diffusion and unitary quantum evolution. By equipping the walker with an internal degree of freedom and a tunable chirality parameter,  $p$ , we interpolate between a standard diffusive random walk and a deterministic, topologically non-trivial quantum walk. We show that the topological protection characteristic of the unitary limit ( $p = 1$ ) remarkably persists into the dissipative regime ( $p < 1$ ). This correspondence allows us to theoretically ground the robustness of edge flows in classical chiral systems using the bulk-boundary correspondence of Floquet topological insulators. Our results provide a discrete microscopic description for odd diffusion, offering a powerful toolkit to predict transport in confined geometries and disordered chiral media.

*Introduction.* The problem of a discrete random walk was introduced by the famous *drunkard's walk* in an exchange of letters between Pearson and Strutt, better known as Lord Rayleigh, in three consecutive volumes of *Nature* in 1905 [1–3]. In the third letter, Pearson concluded that “*the most probable place to find a drunken man (...) is somewhere near his starting point*” [3]. A full, formal solution of the random walk was already provided two months after the original problem statement by Kluyver [4]. The random walk problem was independently used in the early theory of diffusion; both Einstein [5] and Smoluchowski [6] essentially argued with it in their seminal works, Smoluchowski later also acknowledged the connection to the Pearson problem [7]. Since then, the random walk has proven to be of great historical relevance, guiding developments in polymer theory, percolation theory, and many other fields [8, 9]. The idea of the random walk was generalized to arbitrary dimensions [10] or, more recently, led to anomalous diffusion when considering arbitrary jump size and length distributions [11]. In 1993, Aharonov *et al.* [12] broke the classical paradigm within the random walk model by introducing the *quantum random walk*, which harnesses quantum interference through unitary evolution, utilizing an internal degree of freedom (IDF) to facilitate the superposition, for a review see [13].

Much to our surprise, however, a rather fundamental property of physical systems remains almost overlooked in the literature—chiral random walks. Chirality in motion typically originates from a broken parity or time-reversal symmetry of the underlying process and predominantly appears for living microorganisms. Already in 1901, Jennings noted “*On the significance of*

*the spiral swimming of organisms*” [14], a topic that in recent years also has attracted the interest of physicists [15, 16]. Investigations range from artificial colloidal systems [17, 18], over self-propelled chiral agents—bacteria and algae [19–22] to quasi-continuous chiral fluids [23]. Chirality, however, does not only emerge within active systems. Further, external fields can break the time-reversal symmetry and thus give rise to typical chiral behaviour of the tracer particles. The paradigmatic example is a magnetic field to which dipolar agents react in the perpendicular plane, and when the field is rotated, they form chiral colloidal fluids [24, 25]. If the colloidal particles instead carry a charge, the magnetic field induces a Lorentz force, which eventually also results in chiral trajectories of the agents [26–28]. Notably, Lorentz forces in colloidal matter have recently found a renewed interest in the coarse-grained description of skyrmionic spin vortex structures that follow the same time-evolution in the overdamped limit [29, 30].

In the most recent years, these seemingly different systems have found a unifying terminology and started to be investigated from a joint perspective. There, chiral motion is described in terms of transport tensors with anti-symmetric off-diagonal elements. These elements behave odd under inverting the direction of chirality, which has become the namesake for such *odd* systems. In two spatial dimensions, oddness does not conflict with isotropy and in fact, odd transport tensor represent the most general isotropic description of a system [31]. Chiral fluids, for example, are described by odd viscosity on the continuum level [32], networks with transverse forces (a local source of chirality) are described by odd elasticity [33]. On the discrete level, chiral agents perform odd-diffusive motion [34–36] and react with odd mobility to forces in the system [37–39]. Despite the efforts on the continuous description of chiral processes, little work has been done on a discrete, chiral random walk (CRW) model. To our

\* [jan.wojcik@phdstud.ug.edu.pl](mailto:jan.wojcik@phdstud.ug.edu.pl)

† [erik.kalz@uni-potsdam.de](mailto:erik.kalz@uni-potsdam.de)

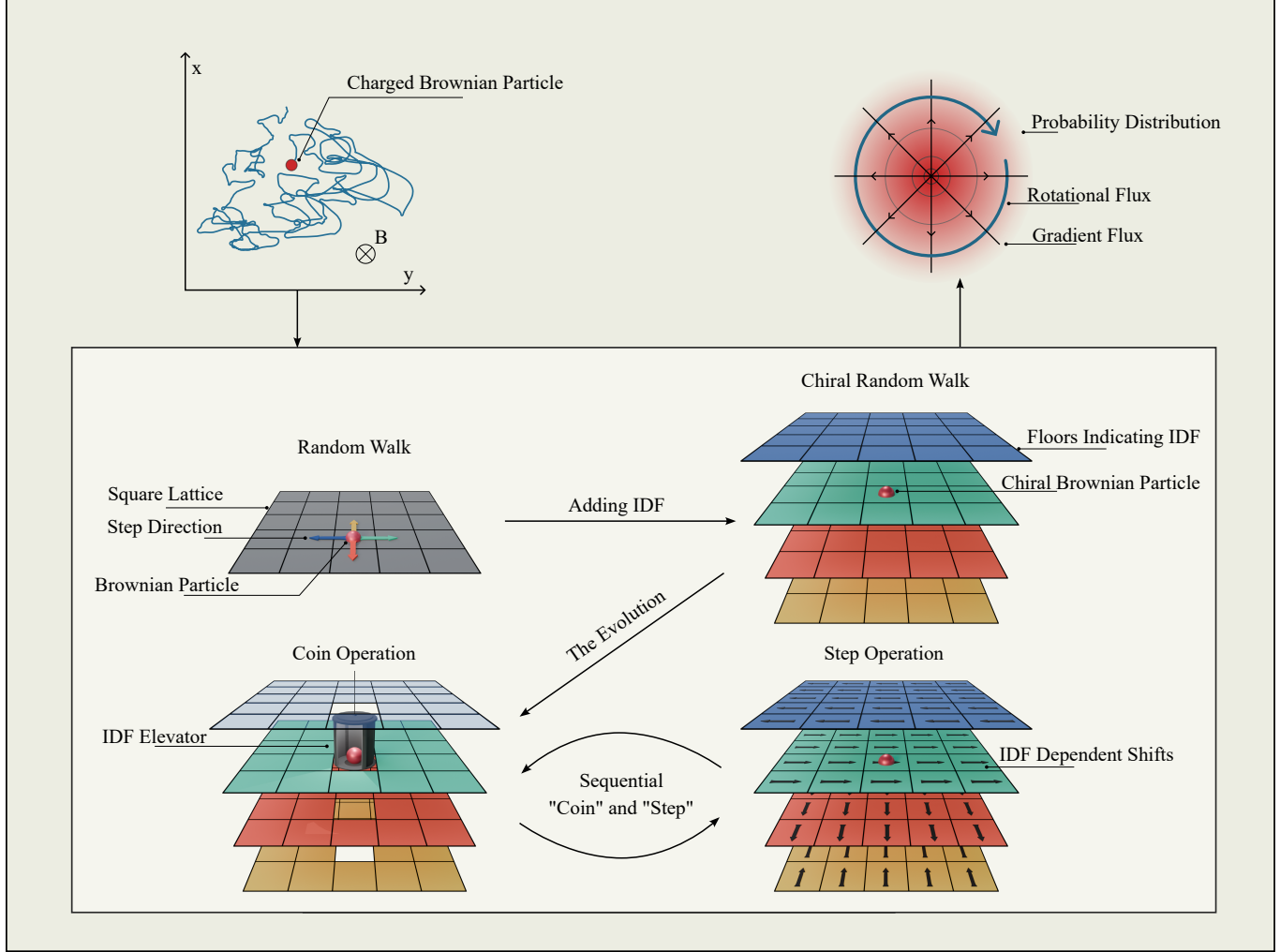


**FIG. 1. Conceptual scheme of the chiral random walk model.** A charged Brownian particle in a magnetic field experiences Lorentz forces that induce chiral motion. Its diffusive motion, however, cannot be captured by a standard random walk model on a lattice. To model such systems, we introduce an internal degree of freedom (IDF), represented schematically as floors in a building. The time evolution then decomposes into two sequential operations: the coin operation, which acts on the IDF, similar to a lift between the floors, while the step operation shifts the particle's position on the lattice according to which floor, i.e., which IDF state ( $\rightarrow, \leftarrow, \uparrow, \downarrow$ ), it currently has. This structure enables the model to incorporate passive chirality, resulting in a probability distribution that exhibits not only standard gradient flux but also rotational flux, the hallmark of odd diffusion that cannot be reproduced by classical random walks.

knowledge, only active chirality has been dealt with from a discrete perspective, with the intrinsic feature that chirality was represented by a drift preference and thus requires a nonequilibrium setting of an active walker [34]. The difficulty in relaxing that property can be illustrated by considering the process of overdamping the Brownian particle with Lorentz force [40–42], a prototypical passive chiral process. The broken time-reversal symmetry on the velocity process, as induced by the magnetic field, has to be accounted for in the limit of vanishing inertia—which is precisely what the antisymmetric odd-diffusion tensor does. However, the price is a Gaussian, but non-white noise, which inherits the broken time-reversal symmetry in its fluctuations [40]. That, however, can hardly

be understood from a discrete perspective: the seemingly intuitive way to include chirality via an orthogonal bias in the step fails for an arbitrary chirality [43].

Chiral systems, active and passive, have a surprising property. While in the bulk, the dynamics of an odd-diffusive tracer appear divergence-free and virtually indistinguishable from ordinary diffusion, when boundaries are introduced, persistent edge flows emerge. These edge flows are not only remarkably robust against disorder [44, 45], but have started to become an experimental indicator of chirality [23, 24, 46–48]. This robustness has prompted an analogy with topological phenomena in quantum systems, where the celebrated bulk-boundary correspondence guarantees protected edge transport [49].

Consequently, efforts have been directed toward connecting odd systems to the quantum Hall effect [44, 50, 51], thereby opening the door to applying the extensive toolkit developed in quantum mechanics to analyse topological behaviour in classical, dissipative settings. A growing body of both theoretical and experimental work has strengthened this connection [52, 53], often by mapping steady-state solutions of dissipative systems to zero-energy eigenstates of quantum Hamiltonians with non-trivial topological invariants [54]. Establishing such mappings is far from trivial, as dissipative dynamics are inherently probabilistic, in contrast to the deterministic evolution of closed quantum systems. Nevertheless, once a reliable mapping is achieved, the predictive power of quantum theory can be harnessed to explain, and even anticipate, complex features of odd systems, such as robust edge transport.

In this work, we introduce a discrete random walk model for a (passive) chiral tracer that captures the essential features of odd diffusion. To achieve this, we adopt the concept of an IDF, akin to that used in discrete-time quantum walks. This IDF acts as a directional guide for the particle's motion. Crucially, the evolution is governed by a single parameter  $p$  ( $0 \leq p \leq 1$ ) that interpolates between stochastic and deterministic dynamics. At one extreme, when  $p = 0$ , we recover the classical random walk. For  $0 < p < 1$ , the walker shows the characteristics of a chiral tracer with odd diffusion. At the other extreme, for  $p = 1$ , the dynamics becomes fully deterministic. As such, it is governed by a bistochastic, unitary evolution matrix and can be mapped to a quantum walk. The latter allows us to apply quantum mechanical tools, and specifically enables us to probe the emergence of topologically protected edge transport in chiral, diffusive systems.

*Model.* We outline the model by starting to construct the random walk on a square lattice  $a\mathbb{Z}^2$ , where  $a$  is the lattice constant, that we set to one for simplicity. The time evolution is discrete, with integer multiples of the unit timescale  $\tau$ , which we also set to one. At time-step  $t$ , the walker has a position  $\mathbf{X}_t = (X_t, Y_t) \in \mathbb{Z}^2$ . We denote by  $p_{\mathbf{x}}(t)$  the probability of the walker to be at position  $\mathbf{X}_t$ , at time  $t$ , i.e.,  $p_{\mathbf{x}}(t) = \text{Prob}\{\mathbf{X}_t = \mathbf{x}\}$ . The probability vector, akin to the probability amplitude vector in quantum mechanics, can be written as

$$|\rho(t)\rangle = \sum_{\mathbf{x}} p_{\mathbf{x}}(t) |\mathbf{x}\rangle, \quad (1)$$

where  $|\mathbf{x}\rangle = |x\rangle|y\rangle$  are the spatial basis eigenvectors, e.g.,  $|x = 0\rangle = (1, 0, \dots, 0)^T$  where  $(\cdot)^T$  denotes the usual matrix transposition.

The discrete-time random walk evolves in finite steps according to

$$|\rho(t+1)\rangle = U|\rho(t)\rangle \quad (2)$$

where  $U$  is the stochastic evolution operator. In the standard random walk,  $U$  shifts the tracer to nearest-

neighbour positions with equal probability

$$\begin{aligned} U|\rho(t)\rangle &= \sum_{\mathbf{x}} p_{\mathbf{x}}(t) U|\mathbf{x}\rangle \\ &= \sum_{\mathbf{x}} \sum_{\sigma} p_{\mathbf{x}}(t) \frac{1}{4} |\mathbf{x} + \sigma\rangle, \end{aligned} \quad (3)$$

where  $\sigma = (\sigma_x, \sigma_y)$  and  $\sigma_i \in \{+1, -1\}$ ,  $i = x, y$ .

This time evolution resembles Markovian dynamics, as after each time step, the information about the previous position of the tracer is lost [9]. To generalize this model to include chirality, this introduces a conceptual difficulty, as one step should introduce a bias for the next one. For example, in clockwise chiral motion, a step to the right should increase the probability of a subsequent downward step.

For the CRW, we have to extend the state of the particle with an IDF  $\mathcal{D} \in \{\rightarrow, \leftarrow, \uparrow, \downarrow\}$ . The full-time evolution of the process acts on the product-space  $\mathbb{Z}^2 \otimes \mathcal{D}$ . The probability of finding the particle at position  $\mathbf{X}_t$  with internal degree  $\mathcal{D}_t$  at time  $t$  now is the joint probability  $p_{\mathbf{x}, d}(t) = \text{Prob}\{\mathbf{X}_t = \mathbf{x}, \mathcal{D}_t = d\}$ . Note that marginalizing the internal degree gives the previous probability  $p_{\mathbf{x}}(t) = \sum_d p_{\mathbf{x}, d}(t)$ . The probability vector now incorporates the internal degree via

$$|\rho(t)\rangle = \sum_{\mathbf{x}, d} p_{\mathbf{x}, d}(t) |\mathbf{x}\rangle \otimes |d\rangle. \quad (4)$$

The four basis vectors of  $\mathcal{D}$  are given by  $|\rightarrow\rangle = (1, 0, 0, 0)^T$ ,  $|\leftarrow\rangle = (0, 1, 0, 0)^T$ ,  $|\uparrow\rangle = (0, 0, 1, 0)^T$ ,  $|\downarrow\rangle = (0, 0, 0, 1)^T$ . We also denote the product state as  $|\mathbf{x}, d\rangle$ .

Inspired by the time-evolution in the quantum walk model [13], which also utilizes an IDF, we propose a decomposition of  $U$  as

$$U = S(I \otimes C), \quad (5)$$

which is a product of a step operator  $S$  that accounts for the topological structure of the lattice, and a coin operator  $C$  that governs the transition probabilities between internal states. The identity  $I$  here acts on the spatial dimensions. The step operator  $S$  is a conditional permutation matrix that shifts the particle according to its internal state. For the nearest-neighbour walk on the square lattice that we consider here, the four possible steps are given by

$$S|x, y, \rightarrow\rangle = |x+1, y, \rightarrow\rangle, \quad (6a)$$

$$S|x, y, \leftarrow\rangle = |x-1, y, \leftarrow\rangle, \quad (6b)$$

$$S|x, y, \uparrow\rangle = |x, y+1, \uparrow\rangle, \quad (6c)$$

$$S|x, y, \downarrow\rangle = |x, y-1, \downarrow\rangle. \quad (6d)$$

The coin operator  $C$  determines the transition probabilities and is a stochastic  $4 \times 4$  matrix in our case, given by

$$C_{\text{rand}} = \frac{1}{4} \begin{pmatrix} 1 & 1 & 1 & 1 \\ 1 & 1 & 1 & 1 \\ 1 & 1 & 1 & 1 \\ 1 & 1 & 1 & 1 \end{pmatrix}. \quad (7)$$

This choice resembles the time-evolution of Eq. (3) as it randomizes the internal state after each step. In general,  $C$  can also be position-dependent (such that in Eq. 5  $I \otimes C \rightarrow \sum_{\mathbf{x}} |\mathbf{x}\rangle \langle \mathbf{x}| \otimes C_{\mathbf{x}}$ ), to account for spatial inhomogeneities or boundaries in the system. For example, we can model a reflective boundary condition as introduced by a hard wall by setting the  $C_{\mathbf{x}}$  at the boundaries to

$$C_{\text{refl}} = \begin{pmatrix} 0 & 1 & 0 & 0 \\ 1 & 0 & 0 & 0 \\ 0 & 0 & 0 & 1 \\ 0 & 0 & 1 & 0 \end{pmatrix}. \quad (8)$$

We can now use this internal state of the walker to implement a stochastic chiral walk. To gain intuition, we start by demonstrating that a fully deterministic clockwise walk,

$$\begin{array}{ccc} |x, y, \rightarrow) & \longrightarrow & |x+1, y, \downarrow) \\ |x, y-1, \uparrow) & \longleftarrow & |x+1, y-1, \leftarrow) \end{array}, \quad (9)$$

can be obtained by a coin operator of the form

$$C_{\text{chir}} = \begin{pmatrix} 0 & 0 & 1 & 0 \\ 0 & 0 & 0 & 1 \\ 0 & 1 & 0 & 0 \\ 1 & 0 & 0 & 0 \end{pmatrix}. \quad (10)$$

We are now in the position to introduce the *chiral random walk*, which combines the classical random walk model, obtained by a fully mixing coin operator  $C_{\text{rand}}$  of Eq. (7) with probability  $1 - p$ , with the chiral coin  $C_{\text{chir}}$  of Eq. (10), with probability  $p$ , where  $0 \leq p \leq 1$ . The CRW coin thus takes the form

$$C_{\text{CRW}} = \frac{1-p}{4} \begin{pmatrix} 1 & 1 & 1 & 1 \\ 1 & 1 & 1 & 1 \\ 1 & 1 & 1 & 1 \\ 1 & 1 & 1 & 1 \end{pmatrix} + p \begin{pmatrix} 0 & 0 & 1 & 0 \\ 0 & 0 & 0 & 1 \\ 0 & 1 & 0 & 0 \\ 1 & 0 & 0 & 0 \end{pmatrix}. \quad (11)$$

As an example, we consider an initial state  $|\rho(t=0)\rangle = |\mathbf{x} = \mathbf{0}, \rightarrow\rangle$  that evolves after one time step to the state  $|\rho(t=1)\rangle = |x=1, y=0\rangle \otimes (1-p, 1-p, 1-p, 1+3p)^T/4$ . Thus, after a step to the right, for  $p > 0$ , the next step in the downward direction is more probable than any other.

The mean-squared displacement (MSD) of the chiral tracer in the long-time limit can be straightforwardly evaluated (see appendix A) to be Brownian and is given by

$$\text{MSD}(t) = D_0^p t, \quad (12)$$

where  $D_0^p$  is the bare chiral diffusion coefficient, which is given by

$$D_0^p = \frac{a^2}{2\tau} \frac{1-p^2}{1+p^2}. \quad (13)$$

We observe that for  $p \rightarrow 1$  we have  $D_0^p \rightarrow 0$ , which is intuitively clear as the coin operator in Eq. (11) reduces to

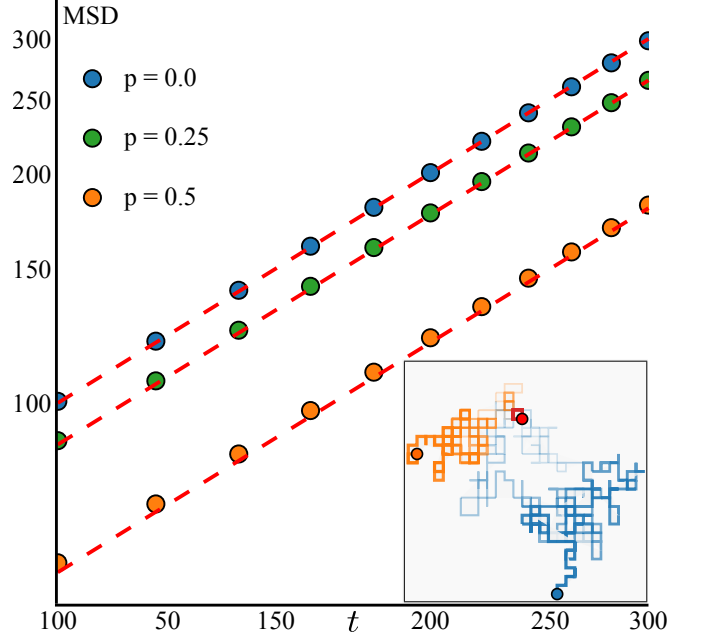


FIG. 2. **MSD of the chiral random walk.** Double-logarithmic plot showing the time dependence of the mean-squared displacement for different values of the chirality parameter  $p$ . The dashed red lines indicate the analytical prediction of Eq. (12), demonstrating excellent agreement with numerical simulations. The inset displays typical trajectories for the standard random walk (blue,  $p = 0$ ), the CRW with intermediate chirality (orange,  $p = 0.5$ ), and the deterministic chiral walk (red,  $p = 1$ ). While all cases ( $p < 1$ ) exhibit Brownian scaling  $\text{MSD} \propto t$ , the bare diffusion coefficient decreases with increasing  $p$  as given by Eq. (13). The  $p = 1$  limit, however, is deterministic and no Brownian motion is observed.

that of Eq. (10) and the motion becomes deterministic, and in circles. In Fig. 2, we compare the long-time MSD of the CRW with Eq. (12) for  $p \in \{0, 0.25, 0.5\}$ . Typical trajectories of the chiral walker and the deterministic limit of  $p = 1$  are shown in the inset.

A characteristic of the CRW is that, despite the isotropy of the system, chirality gives rise to tensorial diffusion. Precisely, chirality introduces so-called *odd diffusion* [34–36] of the walk, which is characterized by antisymmetric off-diagonal elements in the diffusion tensor. Relying on a Green-Kubo formulation for the long-time diffusion [34] (see appendix A), the odd-diffusion tensor of the CRW can be obtained as

$$\mathbf{D} = D_0^p \left( \mathbf{1} + \frac{2p}{1-p^2} \boldsymbol{\epsilon} \right), \quad (14)$$

where  $D_0^p$  is given in Eq. (13),  $\mathbf{1} = \begin{pmatrix} 1 & 0 \\ 0 & 1 \end{pmatrix}$  is the identity tensor, and  $\boldsymbol{\epsilon} = \begin{pmatrix} 0 & 1 \\ -1 & 0 \end{pmatrix}$  is the antisymmetric Levi-Civita symbol in two dimensions. The latter represents the divergence-free elements in the diffusion tensor that are inherently caused by chirality and  $\propto p$ . Odd diffusion naturally appears in the overdamped, diffusive limit of physical systems with inherent chirality. Passive chiral

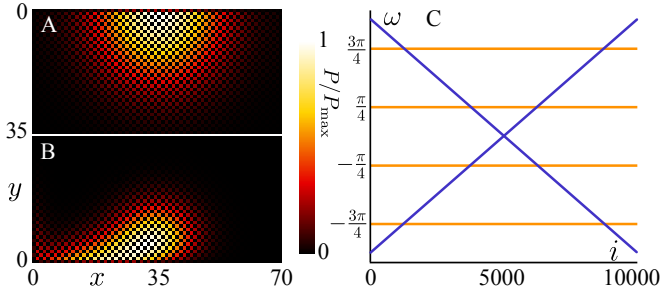


**FIG. 3. Emergence of topological edge modes in the chiral random walk.** (A, B): Heatmaps of probability distribution after 300 steps on a square lattice with reflective boundaries, starting from a near-edge position. (A) Standard random walk ( $p = 0$ ) shows symmetric diffusive spreading. (B) CRW ( $p = 0.7$ ) exhibits pronounced accumulation along the boundary and a characteristic teardrop shape, with the handedness determined by the sign of  $p$ . This edge-following behaviour, absent in the bulk, emerges from the antisymmetric odd-diffusion tensor and persists robustly against perturbations. (C) Numerically obtained quasi-energy spectrum for the CRW in the deterministic limit  $p = 1$  with reflective boundary conditions. The bulk spectrum (orange) is gapped, while boundary-localized states (blue) close this gap, consistent with the bulk-boundary correspondence for Floquet topological insulators. These edge states are absent under periodic boundary conditions, confirming their topological origin.

systems, such as Brownian particles under the effect of Lorentz force [40], as well as active chiral particles [55] all have an emergent diffusive behaviour that is characterized by a tensor of the form of Eq. (14), typically denoted as  $\mathbf{D} = D_0^\kappa (\mathbf{1} + \kappa \boldsymbol{\varepsilon})$ .  $\kappa$  thereby is connected to the physical origin of chirality ( $\kappa \in \mathbb{R}$ , the sign denotes parity), e.g., for Brownian particles under the effect of Lorentz force,  $\kappa$  is given by the ratio of Lorentz force and friction force, for active chiral particles it is the ratio of active chirality to rotational diffusion. With the mapping  $p = (\sqrt{1 + \kappa^2} - 1)/|\kappa|$ , the CRW therefore models such systems on the lattice, and we note that this is only possible by allowing for an IDF of the walker.

As the characteristic antisymmetric part of the odd diffusion tensor in Eq. (14) represents a divergence-free contribution, it does not affect the time-evolution of the random walk in the bulk. The probability distribution function (PDF) remains Gaussian, yet with a modified bare diffusion coefficient  $D_0^p$ , Eq. (13), but virtually indistinguishable from a nonchiral random walker. If spatial isotropy is broken, however, such as due to an obstacle or at a (reflecting) wall, chirality-induced edge-flows emerge, and already on the level of PDFs, the CRW can be distinguished from the ordinary random walk. In Fig. 3 (A, B), we show a normal random walk versus a CRW close to a reflecting wall, where for the latter the handedness of the CRW chooses the direction of the characteristic teardrop shape. Within the CRW, a quantitative description of such edge-flow phenomena becomes possible, as the model provides a natural bridge between a

stochastic and a unitary (quantum) evolution.

We, therefore, recall that in the limit  $p = 1$ , the coin matrix  $C_{\text{crw}}$  reduces to that of the chiral coin in Eq. (10), which specifically has the structure of a permutation matrix. That makes time-evolution not only bistochastic but also unitary  $U^\dagger U = UU^\dagger = I$ . In a translationally invariant systems this is reflected by an (almost) trivial motion: the particle is moving in circles as shown in Eq. (9). In topologically nontrivial systems, however, such time evolution can be linked to an edge-flow behaviour [49, 56, 57]. To illuminate this connection, we therefore now study the behaviour of the CRW in the  $p = 1$  limit.

*Quantum walk.* In the deterministic limit  $p = 1$ , the evolution operator  $U = S(I \otimes C_{\text{chir}})$  of the CRW becomes bistochastic and unitary. Any unitary matrix can be interpreted as the discrete-time evolution operator of a quantum system [58],

$$|\Psi(t+1)\rangle = \mathcal{U}|\Psi(t)\rangle, \quad (15)$$

where in this interpretation of a two-dimensional discrete-time quantum walk, the state of the walker resides in a Hilbert space and can be written as

$$|\Psi(t)\rangle = \sum_{\mathbf{x},d} a_{\mathbf{x},d}(t) |\mathbf{x},d\rangle. \quad (16)$$

Here  $a_{\mathbf{x},d}(t)$  are the probability amplitudes associated with position  $\mathbf{x}$  and internal state (“coin”)  $d$ . The unitarity of  $U$  allows one to define an effective (Floquet) Hamiltonian via

$$H_{\text{eff}} = \frac{i}{T} \log U. \quad (17)$$

Such systems are periodically driven with period  $T$  and are widely studied, especially from a topological point of view [59, 60]. A key feature of Floquet dynamics is that the quasi-energy spectrum of  $H_{\text{eff}}$  is defined only modulo  $2\pi/T$ , which fundamentally alters the classification of topological phases. For example, it is found that topological invariants such as the Chern number can vanish even though the system is not topologically trivial [61].

For a translationally invariant system, it is convenient to work in the quasi-momentum basis  $|\mathbf{k}\rangle = |k_x, k_y\rangle = \sum_{\mathbf{x}} \exp(i\mathbf{k} \cdot \mathbf{x}) |\mathbf{x}\rangle$ . In this basis, the step operator of Eq. (6) acts diagonally on the internal states

$$S|\mathbf{k}, \rightarrow\rangle = e^{-ik_x} |\mathbf{k}, \rightarrow\rangle, \quad (18a)$$

$$S|\mathbf{k}, \leftarrow\rangle = e^{ik_x} |\mathbf{k}, \leftarrow\rangle, \quad (18b)$$

$$S|\mathbf{k}, \uparrow\rangle = e^{-ik_y} |\mathbf{k}, \uparrow\rangle, \quad (18c)$$

$$S|\mathbf{k}, \downarrow\rangle = e^{ik_y} |\mathbf{k}, \downarrow\rangle, \quad (18d)$$

and the full evolution operator  $U$ , therefore, decomposes into  $4 \times 4$  blocks

$$U_{\mathbf{k}} = \begin{pmatrix} 0 & 0 & e^{-ik_x} & 0 \\ 0 & 0 & 0 & e^{ik_x} \\ 0 & e^{-ik_y} & 0 & 0 \\ e^{ik_y} & 0 & 0 & 0 \end{pmatrix}, \quad (19)$$

Given the structure of  $U_{\mathbf{k}}$ , it is convenient to consider two successive time steps  $V_{\mathbf{k}} = U_{\mathbf{k}}^2$ . The double-step operator  $V_{\mathbf{k}}$  becomes block-diagonal and decomposes into two independent sectors characterized by the diagonal momenta  $k_{\nearrow} = k_x + k_y$  and  $k_{\searrow} = k_x - k_y$ . Explicitly,

$$V_{\mathbf{k}} = \begin{pmatrix} V_{k_{\nearrow}} & 0 \\ 0 & V_{k_{\searrow}} \end{pmatrix}, \quad (20)$$

where each block takes the form

$$V_K = \begin{pmatrix} 0 & e^{-iK} \\ e^{iK} & 0 \end{pmatrix}, \quad (21)$$

for  $K \in \{k_{\nearrow}, k_{\searrow}\}$ . This decomposition maps the original two-dimensional quantum walk exactly onto two independent one-dimensional discrete-time quantum walks propagating along the lattice diagonals.

Each one-dimensional block  $V_K$  can be written in standard quantum-walk form,  $V_K = \bar{S}(I \otimes \bar{C})$ , with  $\bar{S}$  acting as a conditional shift and  $\bar{C}$  a unitary coin operator, which in general can be parametrized as

$$\bar{C} = e^{-i\delta} \begin{pmatrix} \cos \theta e^{i\alpha} & \sin \theta e^{i(\alpha+\beta)} \\ -\sin \theta e^{-i(\alpha+\beta)} & \cos \theta e^{-i\alpha} \end{pmatrix}. \quad (22)$$

We give details on the one-dimensional quantum walk in Appendix B. There, we also show that the parameters of the coin operator  $\bar{C}$  of the system at hand are  $\theta = \pm\pi/2$ ,  $\alpha = 0$ ,  $\beta = \pi/2$ ,  $\delta = \pi/2$ . One-dimensional discrete-time quantum walks separate into two families of Hamiltonians with distinct topological phases for  $\theta > 0$  and  $\theta < 0$  [61]. In the present case, such distinct phases originate in the clockwise ( $\theta = \pi/2$ ) or counterclockwise ( $\theta = -\pi/2$ ) CRW, which, therefore, correspond to opposite topological phases.

From the effective Floquet Hamiltonian of the translationally invariant two-dimensional CRW ( $p = 1$ ), Eq. (17), we find four eigenenergies for each quasi-momentum

$$\omega_k \in \left\{ -\frac{3\pi}{4}, -\frac{\pi}{4}, \frac{\pi}{4}, \frac{3\pi}{4} \right\} \quad (23)$$

The spectrum is gapped in the bulk but, as dictated by the bulk-boundary correspondence for Floquet systems, must close in the presence of boundaries [61]: When translational symmetry is broken by reflective boundaries as we are introducing them via a special coin for the boundary layer, Eq. (8), the quasi-energy gap closes through states localized at the system's edges. These states are topologically protected Floquet edge modes and are directly responsible for the persistent boundary currents observed in the deterministic chiral walk. This behaviour is numerically confirmed in Fig. 3C, where we show that boundary-localised states close the otherwise gapped quasi-energy spectrum, as can be found, in contrast, with periodic boundary conditions. To present the robustness of these states, in Fig. 5 we visualize the CRW for a system where the  $p$  value is randomly chosen at each lattice site; the edge states persist.

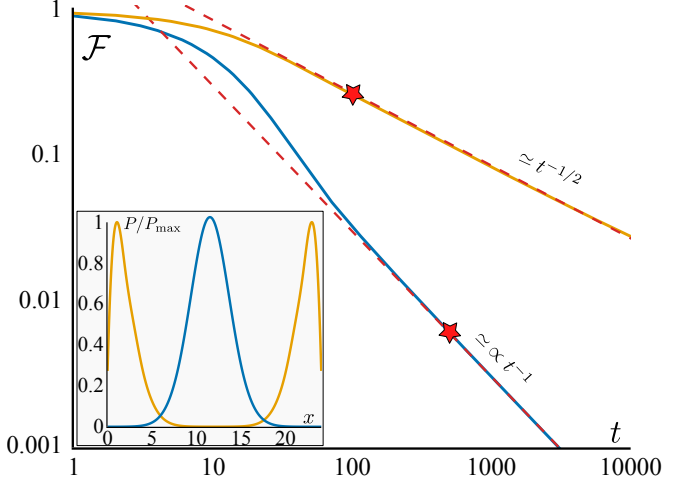


FIG. 4. **Edge and bulk states fidelity decay.** Double-logarithmic plot of the fidelity between the initial probability distribution and the distribution after  $t$  steps of CRW evolution with  $p = 0.9$  on a two-dimensional grid with reflective boundary conditions (system size  $L = 500$ ). We compare two scenarios: an initial state taken as an edge eigenvector of the  $p = 1$  evolution operator (orange) and a bulk eigenvector (blue). Edge states decay as  $\simeq t^{-1/2}$ , characteristic of effectively one-dimensional diffusion, while bulk states decay faster as  $\simeq t^{-1}$ , reflecting two-dimensional spreading. Red stars mark the transition from exponential to polynomial decay. Topologically protected edge states remain long-lived even in the dissipative regime  $p < 1$ . The inset shows the marginal probability distribution summed along one lattice direction (system size  $L = 25$  for visibility) after 100 steps for illustration purposes of the initial states.

For  $p < 1$ , the unitarity of  $U$  is lost, and the evolution becomes non-Hermitian. Consequently, the topological edge states are no longer exact eigenstates of the dynamics. Nevertheless, their signatures persist as long-lived modes which decohere more slowly than the bulk states [62]. To view the populations of these states we compute the fidelity

$$\mathcal{F}(t) = \left( \sum_{\mathbf{x}} \sqrt{p_{\mathbf{x}}(0)p_{\mathbf{x}}(t)} \right)^2. \quad (24)$$

As we show in Fig. 4, initial states localized on topological edge modes exhibit a decay  $\mathcal{F}(t) \simeq t^{-1/2}$ , whereas bulk states decay as  $\mathcal{F}(t) \simeq t^{-1}$  as  $t \gg 1$ . A localized state initially decays exponentially until the system occupies all near-edge/bulk states, and is followed by a quasi one-dimensional random walk with decay  $\propto t^{-1/2}$  for the edge state that effectively cuts the dimensionality or by a regular two-dimensional random walk with decay  $\propto t^{-1}$  in the bulk [62]. We conclude that the ubiquitous phenomenon of robust edge modes in odd (chiral) systems [23, 24, 44–48] cannot only be studied in the CRW model but also understood from the perspective of topologically protected states in unitary systems.

*Applications.* In quantum walks, it is well established

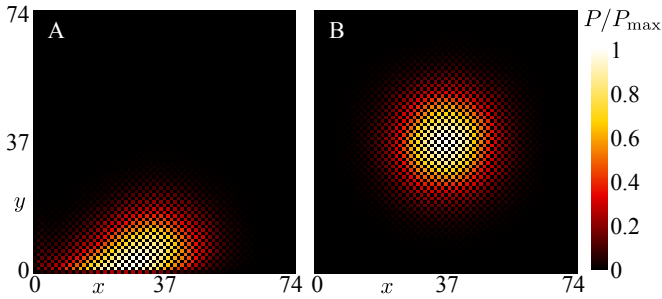


**FIG. 5. Robust topological edge modes in chiral random walk with spatially disordered chirality parameter.** Heatmaps of probability distribution after 300 steps of the CRW on a square lattice, where the chirality parameter  $p$  is randomly chosen from the interval  $[0.1, 0.9]$  at each lattice site. Initial conditions are (A) near-edge position and (B) centre position. Despite the strong spatial disorder in  $p$ , the bulk behaviour remains diffusive and qualitatively unchanged, while edge currents show robustness against local variations in chirality strength, consistent with the topological protection hypothesis.

that topologically protected edge states form at interfaces between regions with distinct topological phases [57]. To explore whether this phenomenon carries over to the CRW, we construct a system that contains two regions; in the upper half, we impose a counterclockwise CRW, while in the lower half, it is clockwise. In the deterministic limit, these two configurations correspond to opposite topological phases. Figure 6 shows that indeed particles preferentially accumulate at the interface between the opposite chirality regions and follow its path, a phenomenon previously observed in odd systems [63, 64]. This behaviour persists despite the absence of any physical barrier at the interface, demonstrating that the topological character of the edge states survives into the dissipative regime.

Having established the topological origin of edge currents in the CRW, we now examine whether these edge states offer practical advantages for transport. In quantum walks, topological edge states are known to optimize transport efficiency in certain geometries [57]. To test whether also this phenomenon carries over to the CRW, we consider a system with uniform chirality ( $p = 0.8$ ) and introduce randomly distributed reflective obstacles on the lattice, as shown in Fig. 7 C. These obstacles mimic a porous material, with reflection implemented through the reflective coin operator of Eq. (8) at predetermined positions. The results, presented in Fig. 7 A and B, reveal a marked advantage of chiral motion: the chiral walker (Fig. 7 B) spreads significantly faster through the disordered medium than the standard random walker (Fig. 7 A). This enhanced transport can be attributed to the edge-following behaviour, which allows the chiral tracer to navigate around obstacles more efficiently. Remarkably, we find that transport is enhanced even further when the reflective obstacles are replaced by regions of opposite chirality (Fig. 7 D). In this configura-

tion, the interface currents discussed in Fig. 6 appear to guide the particle along the boundaries of the heterochiral regions, creating effective transport channels through the disordered landscape. While these examples represent preliminary explorations, they demonstrate the predictive power of the CRW model and suggest promising avenues for discovering new transport phenomena in odd systems. The ability to tune chirality locally opens possibilities for engineering transport pathways in soft matter and colloidal systems without relying on external fields or confinement.

*Conclusions.* We have established the CRW as a minimal microscopic model that captures the essential phenomenology of odd diffusion while providing a direct bridge to topological quantum walks. By introducing an IDF to the classical random walk and a single tuneable parameter  $p$ , we interpolate continuously between standard diffusive motion ( $p = 0$ ) and deterministic, topologically nontrivial quantum walks ( $p = 1$ ).

The central finding of this work is that the topological protection characteristic of the unitary limit persists remarkably into the dissipative regime. Edge currents in chiral systems, previously understood primarily through continuum hydrodynamics, emerge naturally in our discrete framework as manifestations of Floquet topologi-

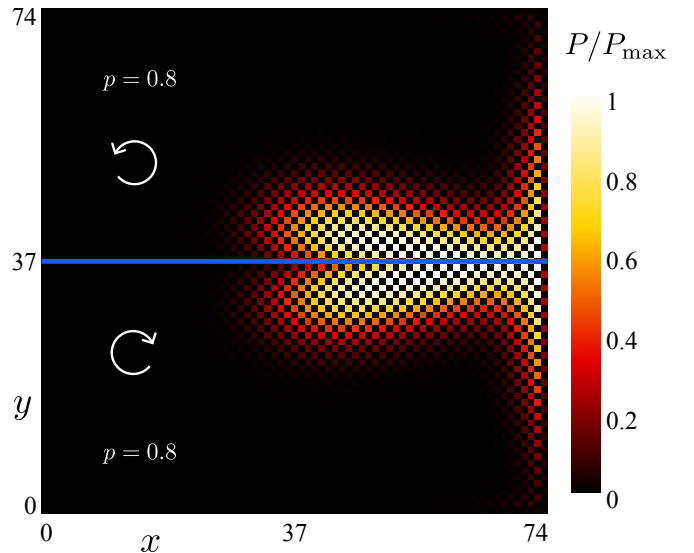


**FIG. 6. Topological interface currents between heterochiral domains.** Heatmap of probability distribution after 300 steps of the CRW in a system divided into two regions with opposite chirality. For  $y < 37$ , clockwise chirality with  $p = 0.8$ ; for  $y \geq 37$ , counterclockwise chirality with  $p = -0.8$  (separated by the blue line). The initial probability distribution was symmetrically placed at two vertices near the interface between opposite chirality regions. Reflective boundaries were imposed at the system edges. Particles accumulate along the interface and follow its path, despite the absence of a physical barrier, demonstrating that topological edge states form at the boundary between regions of opposite topological phase.

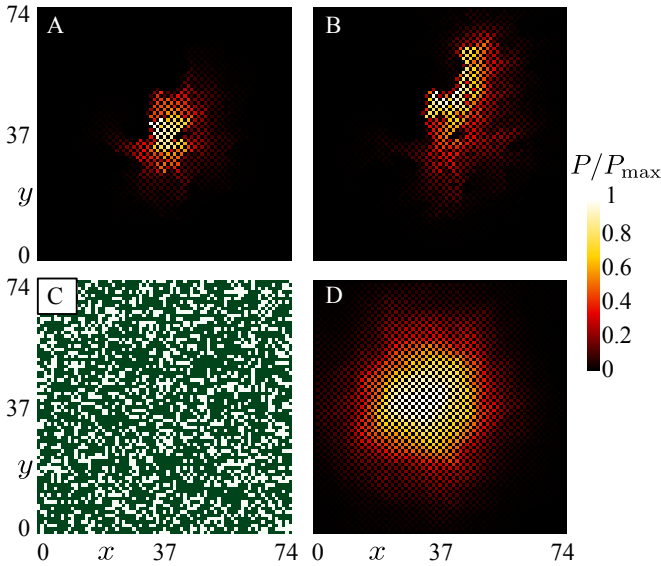


**FIG. 7. Enhanced transport in disordered media via chiral edge modes** (A, B, D): Heatmaps of probability distribution after 500 steps starting from the centre of a square lattice. (A) Standard random walk and (B, D) CRW ( $p = 0.8$ ) in the presence of disorder. In panels (A) and (B), reflective coins are placed at positions marked by white squares in panel (C), modelling a porous medium. The chiral walker (B) exhibits significantly faster spreading than the standard random walker (A), demonstrating enhanced transport through edge-following behaviour. In panel (D), the reflective obstacles are replaced with regions of opposite chirality (counterclockwise,  $p = -0.8$ ) at the same positions. This configuration shows even more pronounced spreading, as interface currents along heterochiral boundaries create effective transport channels. (C) Random pattern of obstacle positions (white squares) used in panels (A), (B), and (D).

cal edge states. This connection is more than a formal analogy: the bulk-boundary correspondence of quantum systems provides quantitative predictions for the robustness and decay properties of edge modes for classical odd-diffusive tracers. Even in the presence of dissipation ( $p < 1$ ) and spatial disorder, edge states decay as  $\simeq t^{-1/2}$ , significantly slower than bulk modes, which follow  $\simeq t^{-1}$ , directly reflecting the spectral structure of the underlying effective Hamiltonian.

Beyond theoretical unification, the CRW offers practical predictive power for complex transport scenarios. Our simulations demonstrate enhanced diffusion through porous media and the emergence of interface currents between heterochiral domains—phenomena that would be challenging to anticipate from hydrodynamic equations alone. The local tunability of chirality in the model suggests new design principles for transport control in soft matter systems. For instance, patterned regions of opposite chirality could serve as transport channels, guiding particles along predetermined paths without physical confinement or external forcing.

The correspondence we have established allows the ex-

tensive toolkit of topological band theory to be harnessed for classical dissipative systems. Questions about transport in complex geometries, the role of quenched disorder, or the effects of heterogeneous chirality patterns can now be addressed through well-established quantum mechanical methods. This opens pathways for the rational design of chiral colloidal devices and active matter systems with engineered transport properties.

Looking forward, the CRW model invites experimental validation in systems where local chirality can be controlled, such as colloidal particles in rotating magnetic fields or active matter with tunable chirality [65]. Extensions to other lattice geometries [66, 67], or the incorporation of self-propulsion [68], interactions between multiple walkers [69], or obstacles and disorder [70–72] represent natural next steps. The framework may also prove valuable in understanding topological phenomena in other non-Hermitian classical systems [73, 74], where the interplay between topology and dissipation remains an active frontier.

*Acknowledgments.* J. W. acknowledges support by the Narodowe Centrum Nauki (OPUS grant No. 2024/53/B/ST2/04103). We acknowledge fruitful discussions with Abhinav Sharma, Ralf Metzler and Antoni Wójcik.

## DATA AVAILABILITY STATEMENT

The data that support the findings of this article are openly available at [75]

## Appendix A: Odd diffusion tensor

The (chiral) random walk follows a discrete-time evolution with timestep  $\tau$  on a two-dimensional square lattice  $a\mathbb{Z}^2$ , where  $a$  is the lattice constant. The internal (coin) space  $\mathcal{D}$  has  $z$  states labelled by  $d = 1, \dots, z$ .

Each coin state is associated with a unit displacement vector  $\mathbf{e}_d \in \mathbb{R}^2$  that points to the lattice neighbour reached when the walker is in coin state  $d$ . The time-evolution  $U$  of the random walk can be decomposed as  $U = S(I \otimes C)$  into a coin operator (a classical stochastic matrix)  $C \in \mathbb{R}^{z \times z}$ , and a conditional step operator  $S$  which moves the walker by  $a\mathbf{e}_d$ . The coin chain is a Markov Chain with transition matrix  $C$ . Assume  $C$  is irreducible and aperiodic, so it has a unique stationary distribution  $\boldsymbol{\pi}$  satisfying  $C\boldsymbol{\pi} = \boldsymbol{\pi}$ . Following Ref. [76], we can write the diffusion tensor via a discrete analogue of the Green-Kubo formula as

$$\mathbf{D} = \frac{a^2}{2\tau} \frac{1}{2} \left[ \mathbf{C}_v(0) + 2 \sum_{t=1}^{\infty} \mathbf{C}_v(t) \right], \quad (\text{A1})$$

where  $\mathbf{C}_v(t) = \langle (\mathbf{v}_0 - \bar{\mathbf{v}}) \otimes (\mathbf{v}_n - \bar{\mathbf{v}})^T \rangle$  is the velocity autocorrelation tensor and  $\mathbf{v}_t$  is the walker's “velocity” at step  $t$ ,  $\mathbf{v}_t = \mathbf{e}_{d_t}$ , where  $d_t$  is the coin state at time  $n$ .

Further,  $\bar{\mathbf{v}} = \sum_d \pi_d \mathbf{e}_d$  is the stationary mean velocity, i.e.,  $\bar{\mathbf{v}} = \mathbf{0}$  in the unbiased case.  $\langle \cdot \rangle$  denotes expectation in the stationary measure. Note that  $\mathbf{C}_v(0) = \mathbf{1}$ .

Because the coin chain is Markov, the joint distribution of  $(d_0, d_t)$  at stationarity is  $\text{Prob}\{d_0 = i, d_t = j\} = \pi_i [C^t]_{ij}$ . The velocity autocorrelation tensor in the unbiased case is thus given by

$$\mathbf{C}_v(t) = \sum_{i,j=1}^z \pi_i [C^t]_{ij} (\mathbf{e}_i - \bar{\mathbf{v}}) \otimes (\mathbf{e}_j - \bar{\mathbf{v}})^T. \quad (\text{A2})$$

From here, we can write a numerically convenient form for calculating the diffusion tensor. Define the “lattice-geometry” matrix  $\mathbf{E} \in \mathbb{R}^{2 \times z}$ , whose  $d$ th column is  $\mathbf{e}_d$ . Put the stationary distribution elements on the diagonal as  $\mathbf{\Pi} = \text{diag}(\boldsymbol{\pi})$  and define the centred geometry  $\mathbf{V} = \mathbf{E} - \bar{\mathbf{v}} \mathbf{1}_z^T$ , where  $\mathbf{1}_z$  is the  $z$ -vector of ones. The  $d$ th row of  $\mathbf{V}$  thus represents the centred velocity for the  $d$ th coin degree, i.e.,  $\mathbf{V}_{:,d} = \mathbf{e}_d - \bar{\mathbf{v}}$ . The diffusion tensor of Eq. (A1) thus can be brought into the explicit  $2 \times 2$  form

$$\mathbf{D} = \frac{a^2}{2\tau} \frac{1}{2} \left[ \mathbf{1} + 2 \sum_{t=1}^{\infty} \mathbf{V} \mathbf{\Pi} [C^t]^T \mathbf{V}^T \right]. \quad (\text{A3})$$

Given the basic random walk ingredients of (i), the coin operator  $C$ , from which a stationary vector  $\boldsymbol{\pi}$  can be computed and (ii), the list of lattice geometry vectors  $\{\mathbf{e}_d\}$  (i.e., the conditional step operator  $S$ ), Eq. (A3) thus gives access to the long-time diffusive properties of the walk.

We can specify Eq. (A3) to the CRW on the square lattice with coin operator given by Eq. (11) of the main text. Chirality contributes via a permutation matrix and therefore does not alter the stationary distribution, which is given by  $\boldsymbol{\pi} = (1/4, 1/4, 1/4, 1/4)^T$ . Thus,  $\boldsymbol{\pi}$  is uniform and independent of  $p$ . The square lattice is characterized by the direction vectors  $\mathbf{e}_1 = (1, 0)$ ,  $\mathbf{e}_2 = (-1, 0)$ ,  $\mathbf{e}_3 = (0, 1)$  and  $\mathbf{e}_4 = (0, -1)$  according to the ordering of our coin degrees  $\mathcal{D} = \{\rightarrow, \leftarrow, \uparrow, \downarrow\}$  and the step operator in Eqs. (6a)-(6d). One obtains straightforwardly

$$C_v^{xx}(t) = C_v^{yy}(t) = 2 \cos(t\pi/2) p^t, \quad (\text{A4a})$$

$$C_v^{xy}(t) = 2 \cos((t-1)\pi/2) p^t, \quad (\text{A4b})$$

$$C_v^{yx}(t) = 2 \cos((t+1)\pi/2) p^t, \quad (\text{A4c})$$

from which it follows that

$$D_{xx} = D_{yy} = \frac{a^2}{2\tau} \frac{1-p^2}{1+p^2}, \quad (\text{A5a})$$

$$D_{xy} = -D_{yx} = \frac{a^2}{2\tau} \frac{2p}{1+p^2}. \quad (\text{A5b})$$

## Appendix B: One dimensional discrete time quantum walk

The discrete-time quantum walk describes the dynamics of a particle on a given lattice equipped with an internal degree of freedom, for a review see Ref. [13]. For

a one-dimensional walk, we consider a particle with position  $x \in \mathbb{Z}$  and a two-dimensional internal state space, the so-called coin degree of freedom. The particle’s wave function can be written as

$$|\psi\rangle = \sum_x |x\rangle \otimes (a_x |+1\rangle + b_x |-1\rangle), \quad (\text{B1})$$

where  $a_x$  and  $b_x$  are the probability amplitudes,  $|x\rangle$  denotes the position basis state, and  $|\pm 1\rangle$  represent the coin basis states.

The time evolution of the discrete-time quantum walk is governed by a unitary evolution operator  $|\psi(t+1)\rangle = U|\psi(t)\rangle$ , which we decompose as

$$U = S \left( \sum_x |x\rangle\langle x| \otimes C_x \right), \quad (\text{B2})$$

where  $S$  is the step operator and  $C_x$  is the (in general position-dependent) coin operator. The step operator acts as a state-dependent translation given by

$$S|x, \pm 1\rangle = |x \pm 1, \pm 1\rangle, \quad (\text{B3})$$

while the coin operator performs a unitary transformation on the internal degree of freedom. The most general form of the coin operator can be parametrized as

$$C_x = e^{-i\delta_x} \begin{pmatrix} e^{i\zeta_x} \cos \theta_x & e^{i(\zeta_x + \sigma_x)} \sin \theta_x \\ -e^{-i(\zeta_x + \sigma_x)} \sin \theta_x & e^{-i\zeta_x} \cos \theta_x \end{pmatrix}, \quad (\text{B4})$$

where with real parameters  $\delta_x$ ,  $\zeta_x$ ,  $\sigma_x$ ,  $\theta_x$ .

To make contact with solid-state theory, we introduce an effective Hamiltonian via  $H_{\text{eff}} = i \log U/T$ , with eigenenergies defined through  $U|\psi\rangle = \exp(-i\omega)|\psi\rangle$ . For translationally invariant systems, where the coin operator is position-independent, we work in the quasi-momentum basis  $|k\rangle = \sum_x \exp(-ikx)|x\rangle$  with  $k$  restricted to the first Brillouin zone  $-\pi \leq k \leq \pi$ . In this basis, the step operator acts diagonally as

$$S|k, \pm 1\rangle = e^{\mp ik}|k, \pm 1\rangle, \quad (\text{B5})$$

while the coin operator remains unchanged since it acts only on the internal degree of freedom. We now treat  $\theta$  as a free parameter and define a family of effective Hamiltonians

$$H(\theta) = \oint_{BZ} dk (|k\rangle\langle k| \otimes \bar{H}_k), \quad (\text{B6})$$

where  $\bar{H}_k$  is the  $2 \times 2$  Bloch Hamiltonian. This can be represented as  $\bar{H}_k = \delta I + \omega_k \mathbf{n}_k \cdot \boldsymbol{\sigma}$ , with  $\boldsymbol{\sigma} = (\sigma_x, \sigma_y, \sigma_z)$  denoting the vector of Pauli matrices and the normalized Bloch vector given by

$$\mathbf{n}_k = \frac{1}{\sin \omega_k} \begin{pmatrix} \sin \theta \sin(k - \tau) \\ -\sin \theta \cos(k - \tau) \\ \cos \theta \sin(k - \alpha) \end{pmatrix}, \quad (\text{B7})$$

where  $\tau = \alpha + \beta$ . The quasi-energy  $\omega_k$  satisfies

$$\cos \omega_k = \cos \theta \cos(k - \alpha), \quad (\text{B8})$$

and the eigenenergies are given by  $\omega_{k\pm} = \delta \pm \omega_k$ , with corresponding projectors

$$\rho_{k\pm} = \frac{1}{2}(I + \mathbf{n}_\pm \cdot \boldsymbol{\sigma}), \quad (\text{B9})$$

and  $\mathbf{n}_{k\pm} = \pm \mathbf{n}_k$ .

For the CRW in the deterministic limit  $p = 1$ , we substitute the coin parameters  $\alpha = 0$ ,  $\beta = \pi/2$ , and  $\delta = \pi/2$  (with  $\theta$  remaining a free parameter). This yields the normalized Bloch vector

$$\mathbf{n}_k = \frac{1}{\sin \omega_k} \begin{pmatrix} -\sin \theta \cos k \\ -\sin \theta \sin k \\ \cos \theta \sin k \end{pmatrix}, \quad (\text{B10})$$

and the quasi-energy satisfies

$$\omega_k = \arccos(\cos \theta \cos k), \quad (\text{B11})$$

The eigenenergies of the effective Hamiltonian thus take the form  $\omega_{k\pm} = \pi/2 \pm \omega_k$ .

From this expression, we observe that the spectrum of the effective Hamiltonian can be gapped. Let  $\mathcal{S}$  denote the subset of  $\theta$  for which the Hamiltonian exhibits a spectral gap. This set is a disconnected topological space with partition  $\mathcal{S} = \mathcal{S}_{\theta < 0} \cup \mathcal{S}_{\theta > 0}$ , where  $\mathcal{S}_{\theta < 0} = \{\theta \mid -\pi < \theta < 0\}$  and  $\mathcal{S}_{\theta > 0} = \{\theta \mid 0 < \theta < \pi\}$ . Grudka et al. [77] rigorously proved that  $\mathcal{S}_{\theta > 0}$  and  $\mathcal{S}_{\theta < 0}$  support distinct topological phases, using the notion of homotopic relative maps from the Brillouin zone to the Bloch sphere. For our CRW, the clockwise ( $\theta = \pi/2$ ) and counterclockwise ( $\theta = -\pi/2$ ) configurations therefore correspond to opposite topological phases, which underlie the edge state formation at interfaces between heterochiral domains discussed in the main text.

---

[1] K. Pearson, *Nature* **72**, 294 (1905).  
[2] L. Rayleigh, *Nature* **72**, 318 (1905).  
[3] K. Pearson, *Nature* **72**, 342 (1905).  
[4] J. C. Kluyver, Konink. Akad. Wetenschapp. Amsterdam **8**, 341 (1905).  
[5] A. Einstein, *Ann. Phys.* **322**, 549 (1905).  
[6] M. v. Smoluchowski, *Ann. Phys.* **326**, 756 (1906).  
[7] M. v. Smoluchowski, *Physik. Zeitschr.* **17**, 557 (1916).  
[8] S. Chandrasekhar, *Rev. Mod. Phys.* **15**, 1 (1943).  
[9] B. D. Hughes, *Random Walks And Random Environments*, Vol. 1 (Oxford University Press, 1995).  
[10] G. Pólya, *Math. Ann.* **84**, 149 (1921).  
[11] R. Metzler and J. Klafter, *Phys. Rep.* **339**, 1 (2000).  
[12] Y. Aharonov, L. Davidovich, and N. Zagury, *Phys. Rev. A* **48**, 1687 (1993).  
[13] J. Kempe, *44*, 307 (2003).  
[14] H. S. Jennings, *Am. Nat.* **35**, 369 (1901).  
[15] H. Löwen, *Eur. Phys. J. Spec. Top.* **225**, 2319 (2016).  
[16] B. Liebchen and D. Levis, *Europ. Phys. Lett.* **139**, 67001 (2022).  
[17] F. Kümmel, B. Ten Hagen, R. Wittkowski, I. Buttinoni, R. Eichhorn, G. Volpe, H. Löwen, and C. Bechinger, *Phys. Rev. Lett.* **110**, 198302 (2013).  
[18] M. S. D. Wykes, J. Palacci, T. Adachi, L. Ristroph, X. Zhong, M. D. Ward, J. Zhang, and M. J. Shelley, *Soft Matter* **12**, 4584 (2016).  
[19] P. D. Frymier, R. M. Ford, H. C. Berg, and P. T. Cummings, *Proc. Natl. Acad. Sci. USA* **92**, 6195 (1995).  
[20] E. Lauga, W. R. DiLuzio, G. M. Whitesides, and H. A. Stone, *Biophys. J.* **90**, 400 (2006).  
[21] A. P. Petroff, X.-L. Wu, and A. Libchaber, *Phys. Rev. Lett.* **114**, 158102 (2015).  
[22] K. Drescher, K. C. Leptos, I. Tuval, T. Ishikawa, T. J. Pedley, and R. E. Goldstein, *Phys. Rev. Lett.* **102**, 168101 (2009).  
[23] H. Li, H. Chaté, M. Sano, X.-q. Shi, and H. Zhang, *Phys. Rev. X* **14**, 041006 (2024).  
[24] V. Soni, E. S. Bililign, S. Magkiriadou, S. Sacanna, D. Bartolo, M. J. Shelley, and W. T. M. Irvine, *Nat. Phys.* **15**, 1188 (2019).  
[25] H. Massana-Cid, D. Levis, R. J. H. Hernández, I. Pagónabarraga, and P. Tierno, *Phys. Rev. Res.* **3**, L042021 (2021).  
[26] D. S. Lemons and D. L. Kaufman, *IEEE Trans. Plasma Sci.* **27**, 1288 (1999).  
[27] R. Czopnik and P. Garbaczewski, *Phys. Rev. E* **63**, 021105 (2001).  
[28] J. I. Jiménez-Aquino and M. Romero-Bastida, *Rev. Mex. Fis. E* **52**, 182 (2006).  
[29] R. E. Troncoso and Á. S. Núñez, *Ann. Phys.* **351**, 850 (2014).  
[30] C. Reichhardt, C. J. O. Reichhardt, and M. V. Milošević, *Rev. Mod. Phys.* **94**, 035005 (2022).  
[31] E. J. Dresselhaus, S. Govindjee, and K. K. Mandadapu, arXiv:2508.20055 10.48550/arXiv.2508.20055 (2025).  
[32] M. Fruchart, C. Scheibner, and V. Vitelli, *Annu. Rev. Condens. Matter Phys.* **14**, 471 (2023).  
[33] C. Scheibner, A. Souslov, D. Banerjee, P. Surówka, W. T. M. Irvine, and V. Vitelli, *Nat. Phys.* **16**, 475 (2020).  
[34] C. Hargus, J. M. Epstein, and K. K. Mandadapu, *Phys. Rev. Lett.* **127**, 178001 (2021).  
[35] E. Kalz, H. D. Vuijk, I. Abdoli, J.-U. Sommer, H. Löwen, and A. Sharma, *Phys. Rev. Lett.* **129**, 090601 (2022).  
[36] E. Kalz, H. D. Vuijk, J.-U. Sommer, R. Metzler, and A. Sharma, *Phys. Rev. Lett.* **132**, 057102 (2024).  
[37] A. R. Poggiali and D. T. Limmer, *Phys. Rev. Lett.* **130**, 158201 (2023).  
[38] L. Caprini and U. Marini Bettolo Marconi, *J. Chem. Phys.* **162**, 10.1063/5.0262594 (2025).  
[39] E. Kalz, S. Ravichandir, J. Birkenmeier, R. Metzler, and A. Sharma, *Phys. Rev. E* **10**.48550/arXiv.2503.04544 (2025).  
[40] H.-M. Chun, X. Durang, and J. D. Noh, *Phys. Rev. E* **97**, 032117 (2018).  
[41] H. D. Vuijk, J. M. Brader, and A. Sharma, *J. Stat. Mech.:*

Theory Exp. **2019** (6), 063203.

[42] J.-M. Park and H. Park, Phys. Rev. Res. **3**, 043005 (2021).

[43] K. Hijikata, I. Lubashevsky, and A. Vazhenin, Proc. ISCIE SSS **2015**, 213 (2015).

[44] A. Souslov, K. Dasbiswas, M. Fruchart, S. Vaikuntanathan, and V. Vitelli, Phys. Rev. Lett. **122**, 128001 (2019).

[45] C. B. Caporusso, G. Gonnella, and D. Levis, Phys. Rev. Lett. **132**, 168201 (2024).

[46] X. Yang, C. Ren, K. Cheng, and H. P. Zhang, Phys. Rev. E **101**, 022603 (2020).

[47] Q. Yang, H. Zhu, P. Liu, R. Liu, Q. Shi, K. Chen, N. Zheng, F. Ye, and M. Yang, Phys. Rev. Lett. **126**, 198001 (2021).

[48] A. Nelson, D. M. Lobmeyer, S. L. Biswal, and E. Tang, Phys. Rev. Res. **7**, 023094 (2025).

[49] M. Z. Hasan and C. L. Kane, Rev. Mod. Phys. **82**, 3045 (2010).

[50] A. Souslov, B. C. Van Zuiden, D. Bartolo, and V. Vitelli, Nat. Phys. **13**, 1091 (2017).

[51] X. Lou, Q. Yang, Y. Ding, P. Liu, K. Chen, X. Zhou, F. Ye, R. Podgornik, and M. Yang, Proc. Natl. Acad. Sci. USA **119**, e2201279119 (2022).

[52] S. Shankar, A. Souslov, M. J. Bowick, M. C. Marchetti, and V. Vitelli, Nat. Rev. Phys. **4**, 380 (2022).

[53] K. Sone, Y. Ashida, and T. Sagawa, Nat. Commun. **11**, 5745 (2020).

[54] K. Dasbiswas, K. K. Mandadapu, and S. Vaikuntanathan, Proc. Natl. Acad. Sci. USA **115**, E9031 (2018).

[55] P. L. Muzzeddu, H. D. Vuijk, H. Löwen, J.-U. Sommer, and A. Sharma, J. Chem. Phys. **157**, 134902 (2022).

[56] T. Kitagawa, M. S. Rudner, E. Berg, and E. Demler, Phys. Rev. A **82**, 033429 (2010).

[57] J. K. Asbóth, L. Oroszlány, and A. Pályi, *A Short Course on Topological Insulators. Band Structure and Edge States in One and Two Dimensions*, Lecture Notes in Physics (Springer Cham, 2016).

[58] M. A. Nielsen and I. L. Chuang, *Quantum Computation and Quantum Information: 10th Anniversary Edition* (Cambridge University Press, 2010).

[59] J. Cayssol, B. Dóra, F. Simon, and R. Moessner, **7**, 101 (2013).

[60] M. Sajid, J. K. Asbóth, D. Meschede, R. F. Werner, and A. Alberti, Phys. Rev. B **99**, 214303 (2019).

[61] M. S. Rudner, N. H. Lindner, E. Berg, and M. Levin, Phys. Rev. X **3**, 031005 (2013).

[62] B. A. Bhargava, S. K. Das, L. M. Sieberer, and I. C. Fulga, arXiv:2509.03296 [10.48550/arXiv.2509.03296](https://arxiv.org/abs/2509.03296) (2025).

[63] C. Scholz, M. Engel, and T. Pöschel, Nat. Commun. **9**, 931 (2018).

[64] I. Abdoli, H. D. Vuijk, R. Wittmann, J.-U. Sommer, J. M. Brader, and A. Sharma, Phys. Rev. Res. **2**, 023381 (2020).

[65] J. Mecke, J. O. Nketsiah, R. Li, and Y. Gao, **3**, 20230086 (2024).

[66] S. A. Mallory and A. Cacciuto, J. Am. Chem. Soc. **141**, 2500 (2019).

[67] J. Wang, G. Wang, H. Chen, Y. Liu, P. Wang, D. Yuan, X. Ma, X. Xu, Z. Cheng, B. Ji, et al., Nat. Commun. **15**, 8853 (2024).

[68] M. R. Shaebani, A. Wysocki, R. G. Winkler, G. Gompper, and H. Rieger, Nat. Rev. Phys. **2**, 181 (2020).

[69] J. Mason, C. Erignoux, R. L. Jack, and M. Bruna, **479**, 20230524 (2023).

[70] H. Reinken, D. Nishiguchi, S. Heidenreich, A. Sokolov, M. Bär, S. H. L. Klapp, and I. S. Aranson, Commun. Phys. **3**, 76 (2020).

[71] C. W. Chan, D. Wu, K. Qiao, K. L. Fong, Z. Yang, Y. Han, and R. Zhang, Nat. Commun. **15**, 1406 (2024).

[72] J. Mecke, Y. Gao, and M. Ripoll, Phys. Fluids **37**, 112016 (2025).

[73] Y. Ashida, Z. Gong, and M. Ueda, Adv. Phys. **69**, 249 (2020).

[74] K. Sone, K. Yokomizo, K. Kawaguchi, and Y. Ashida, Rep. Prog. Phys. **89**, 016501 (2026).

[75] J. Wójcik and E. Kalz, Github repository, <https://github.com/JanWojcikPhys/Chiral-Random-Walk> (2026).

[76] T. Gilbert and D. P. Sanders, J. Phys. A **43**, 035001 (2009).

[77] A. Grudka, M. Karczewski, P. Kurzyński, J. Wójcik, and A. Wójcik, Phys. Rev. A **107**, 032201 (2023).